CrystEngComm

COMMUNICATION

View Article Online
View Journal | View Issue

Cite this: *CrystEngComm*, 2015, **17**, 3917

Received 21st March 2015,
Accepted 21st April 2015

DOI: 10.1039/c5ce00572h

www.rsc.org/crystengcomm

Random lasing realized in n-ZnO/p-MgZnO core–shell nanowire heterostructures

Ying-Jie Lu,[ab] Chong-Xin Shan,*[a] Ming-Ming Jiang,[a] Guang-Chong Hu,[ab] Nan Zhang,[ab] Shuang-Peng Wang,[a] Bing-Hui Li[a] and De-Zhen Shen*[a]

Well-aligned ZnO nanowire arrays have been prepared, and p-MgZnO has been deposited onto the nanowires to form core–shell heterostructures. Transmission electron microscopy confirms the formation of n-ZnO/p-MgZnO core–shell nanowire heterostructures. Under injection of a continuous current, random lasing with a threshold current of around 15 mA has been observed from the heterostructures. The low threshold may be due to the relatively high crystalline quality of the ZnO nanowires as well as the carrier confinement in the heterostructures.

Introduction

Random lasing is a lasing phenomenon realized in random media, which has attracted much attention in recent years for its significance in both fundamental research and potential applications in versatile fields, such as in displays, sensing, biological imaging, *etc.*[1–6] Many efforts have been devoted to develop random lasers, and optically pumped random lasers have been reported extensively.[7–13] Realizing electrically pumped lasing has been one of the most challenging issues of random lasers, and zinc oxide (ZnO) has been considered as one of the most active materials for electrically pumped random lasers.[14–19] Although many reports have demonstrated electrically pumped random lasing from ZnO, most of them are realized in metal–insulator–semiconductor (MIS) structures.[15,20–24] It is accepted that in MIS structures, holes are generated *via* an impact ionization process under relatively high bias voltage. However, the generation efficiency of such process is very low. Additionally, the relatively high bias voltage may cause serious heating effects, thus greatly degrading the performance of random lasers. A more efficient way for the generation and injection of holes is to construct p–n junctions, in which electrons and holes can be injected from the n-type and p-type layers into the active layer and recombine radiatively there.[25,26] However, very few reports on ZnO-based electrically pumped random lasing from p–n homojunctions can be found to date,[18,27–29] possibly because reproducible p-type doping of ZnO-based materials is still a challenging issue. If an n-ZnO/p-MgZnO heterostructure can be constructed, in which MgZnO has a wider bandgap, holes can then be injected into ZnO and recombine with the electrons there; thus electrically pumped random lasing may be realized. However, no such report can be found to date.

By employing a lithium–nitrogen codoping method, we have realized reproducible p-type ZnO films, and reliable light-emitting devices that can work continuously for several hours have been demonstrated.[30,31] In this paper, n-ZnO/p-MgZnO core–shell heterostructures have been fabricated by employing ZnO nanowires as the active layer. In these structures, the high crystalline and optical quality of the nanowires may facilitate the occurrence of lasing, and the relatively large surface-to-volume ratio of the nanowires will provide an arena for strong scattering that is necessary for random lasing. Under forward bias, electrically pumped random lasers have been realized, and the threshold is around 15 mA, which is much smaller than the corresponding value realized in ZnO p–n junctions (~40 mA).[18]

Experimental

The ZnO nanowires were grown on *a*-plane sapphire substrates by a metal–organic chemical vapor deposition (MOCVD) technique. The precursors used for the growth were diethylzinc and oxygen, and high-purity (9N) nitrogen was used as the carrier gas to lead the precursors into the growth chamber. Prior to growth, the substrates were treated at 850 °C under 10^{-4} Pa for 60 minutes to remove possible absorbed contaminants. During the growth process, the substrate temperature was kept at 650 °C and the pressure in the MOCVD chamber was kept at 3×10^3 Pa. After two hours of growth, the nanowire samples were loaded into a plasma-assisted molecular beam

[a] *State Key Laboratory of Luminescence and Applications, Changchun Institute of Optics, Fine Mechanics and Physics, Chinese Academy of Sciences, Changchun 130033, China. E-mail: shancx@ciomp.ac.cn, shendz@ciomp.ac.cn*
[b] *University of Chinese Academy of Sciences, Beijing 100049, China*

epitaxy facility (VG V80H) for deposition of the p-type MgZnO layer to form the n-ZnO/p-MgZnO core–shell nanowire heterostructures. The detailed growth conditions for the Li and N codoped p-type MgZnO layer can be found elsewhere.[31–33] Briefly, nitric oxide (NO) and oxygen (O_2) cracked *via* an Oxford Applied Research HD25 radio-frequency (13.56 MHz) atomic source were used as the N dopant and O source, respectively. Metallic zinc, magnesium and lithium contained in individual Knudsen effusion cells were used as Zn, Mg and Li sources. During the growth process, the pressure in the growth chamber was fixed at 2×10^{-5} mbar and the NO and O_2 flow rates were maintained at 0.9 and 1.0 sccm, respectively. The substrate temperature was kept at 650 °C. Metallic Ni/Au and an In layer were deposited onto the p-type MgZnO layers and ZnO nanowires by a thermal evaporation method to form ohmic contacts. The thickness of the Ni and Au films for the Ni/Au electrode is about 30 and 500 nm. The morphology of the ZnO nanowires was characterized using a Hitachi S4800 field-emission scanning electron microscope (SEM). The crystalline properties of the ZnO nanowires and core–shell structures were evaluated by using a Bruker D8 Discover X-ray diffractometer (XRD) with Cu Kα (λ = 1.54 Å) as the radiation source and a JEM-2010 transmission electron microscope (TEM). The electrical properties of the MgZnO layer were measured with a Hall system (LakeShore 7707) under a van der Pauw configuration. Electroluminescence (EL) measurements of the heterostructures were carried out in a Hitachi F4500 spectrometer employing a continuous-wave current as the excitation source.

Results and discussion

Fig. 1(a) and (b) show the plan-view and side-view SEM images of the ZnO nanowires that act as the active layer of the random lasers. One can see that well-aligned nanowires have been grown vertically on the sapphire substrate. The length of the nanowires is around 3.8 μm, and the nanowires taper in diameter from around 150 nm at the base to around 40 nm at the top. The XRD pattern of the ZnO nanowire arrays is shown in Fig. 1(c). Only a peak at 34.4° is visible from the pattern besides the diffraction peak of the sapphire substrate, which can be indexed to diffraction of the (0002) facet of wurtzite ZnO. The dominant (0002) diffraction peak reveals that the nanowires may be grown along the [0001] direction of the wurtzite structure. The X-ray rocking curve of the nanowires is illustrated in the inset of Fig. 1(c), from which a Gaussian peak with a full width at half maximum (FWHM) of around 0.46° can be observed. The phi-scan spectrum of the nanowires is shown in Fig. 1(d), and six peaks with an equal interval of 60° can be defined from the spectrum, indicating the six-fold symmetry of the nanowires.

A typical TEM image of the ZnO nanowires is shown in Fig. 2(a), and the nanowires show a smooth surface, revealing that each nanowire is highly crystallized. Also, one can see the tapered structure of the nanowires clearly from the image. The high-resolution TEM image of an individual ZnO

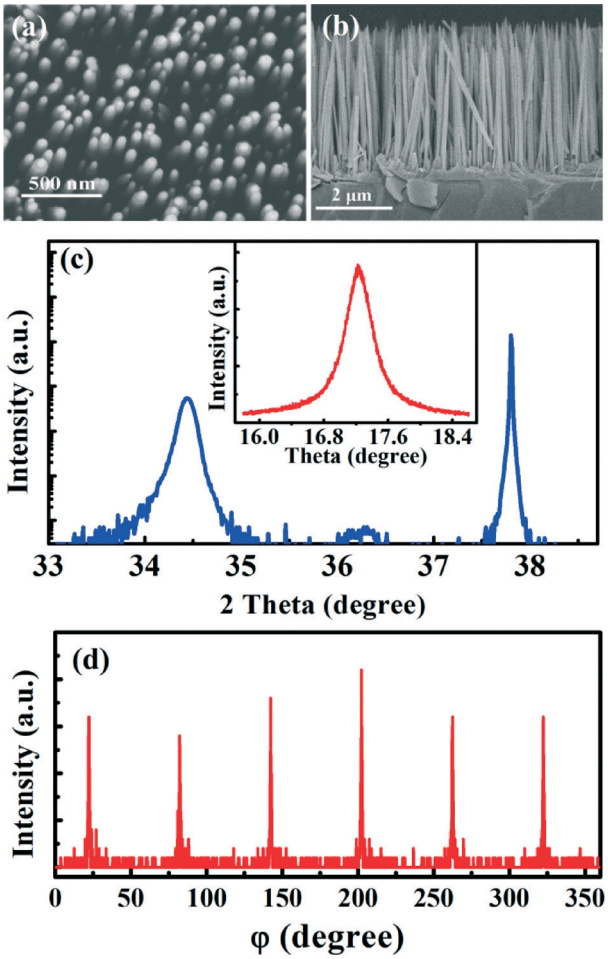

Fig. 1 Plan-view (a) and side-view (b) SEM images of the ZnO nanowires; (c) θ–2θ XRD pattern of the ZnO nanowires (the inset shows the rocking curve of the nanowires); (d) X-ray phi-scan spectrum of the nanowires.

nanowire is shown in Fig. 2(b). Well-defined lattice fringes can be observed, indicating the high crystalline quality of the nanowires. The spacing between two adjacent lattice fringes is around 0.51 nm, which corresponds to the *d*-spacing of the

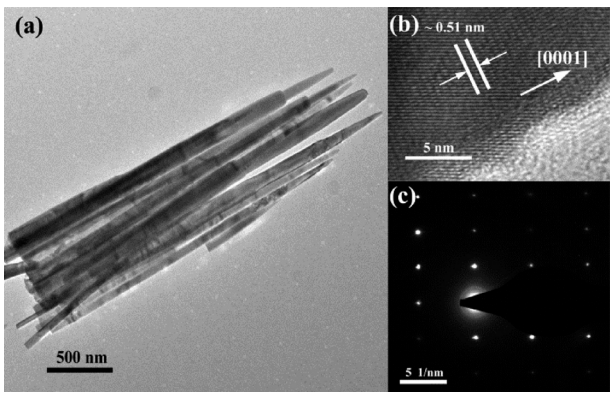

Fig. 2 TEM image of the ZnO nanowires (a); high-resolution TEM image (b) and selected area electron diffraction pattern (c) of an individual ZnO nanowire.

(0001) plane in hexagonal ZnO. From the lattice fringes, one can also see that the nanowires grow along the [0001] direction, which is consistent with the XRD result shown in Fig. 1(c). Fig. 2(c) shows the selected area electron diffraction (SAED) pattern of an individual nanowire. The clear dotted pattern confirms the single-crystalline nature of the nanowires.

To achieve electrically pumped random lasing, p-type MgZnO films have been deposited onto the nanowires to form n-ZnO/p-MgZnO core–shell nanowire heterostructures. The Mg content in the MgZnO layer determined by energy dispersive X-ray spectroscopy (EDS) is 0.35. The electrical properties of the $Mg_{0.35}Zn_{0.65}O$ layers on the nanowires cannot be measured directly by Hall measurement because it will be interfered greatly by the nanowires. Thus, to assess the electrical properties of the $Mg_{0.35}Zn_{0.65}O$ layers, Hall measurements have been carried out on the layers grown directly on the sapphire substrate in the same growth process. The layer shows p-type conduction with a hole concentration of around 9×10^{16} cm^{-3} and a Hall mobility of 0.8 cm^2 V^{-1} s^{-1}. It is then deduced that the $Mg_{0.35}Zn_{0.65}O$ layers deposited onto the ZnO nanowires are p-type conduction. The schematic illustration of the device is shown in Fig. 3(a). The size of the device is 4 mm × 6 mm, as marked in the diagram. The inset of Fig. 3(a) shows the side-view SEM image of the n-ZnO/p-MgZnO core–shell nanowire structure. One can see clearly from the image that the nanowires are grown vertically onto the sapphire substrate with a ZnO layer lying underneath the nanowires. Also, there is a thin MgZnO layer on the top of the nanowires. Fig. 3(b) shows a typical dark field scanning transmission electron microscopy image of an individual n-ZnO/p-$Mg_{0.35}Zn_{0.65}O$ core–shell nanowire heterostructure. One can see from the image that the ZnO nanowire has been coated with a thin $Mg_{0.35}Zn_{0.65}O$ layer to form the core–shell structure. The thickness of the MgZnO shell around the top of the nanowires is about 90 nm. The Zn and Mg elemental mappings of the core–shell structure are shown in Fig. 3(c) and (d). These figures reveal that Zn is mainly concentrated in the core area, while Mg atoms are only distributed within the shell area, which clearly reveals the formation of core–shell heterostructures.

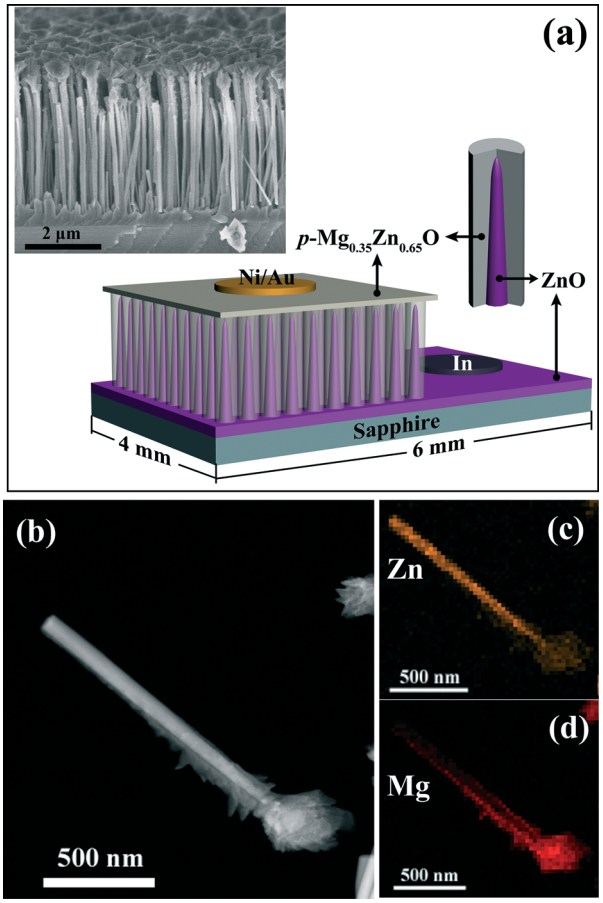

Fig. 3 (a) Schematic diagram of the n-ZnO/p-$Mg_{0.35}Zn_{0.65}O$ core–shell nanowire heterostructure (the inset shows the side-view SEM image of the device); (b) dark field scanning TEM image of an individual ZnO/MgZnO core–shell nanowire heterostructure; EDS elemental mappings of Zn (c) and Mg (d).

The current–voltage (*I–V*) characteristics of the heterostructure show obvious rectification behaviors with a turn-on voltage of around 9.0 V, as shown in Fig. 4(a). The bandgap diagram of the heterostructure is shown in the inset of Fig. 4(a). Under forward bias, the holes in the p-$Mg_{0.35}Zn_{0.65}O$ layer will be drifted into the ZnO nanowires, while the electrons will be confined in the ZnO nanowires because of the barrier formed by the conduction band offset at the ZnO/$Mg_{0.35}Zn_{0.65}O$ interface. The distribution of electrons and holes in the n-ZnO/p-$Mg_{0.35}Zn_{0.65}O$ core–shell heterostructure has been simulated using the finite-difference time-domain (FDTD) method, as shown in Fig. 4(b) and (c). One can find that electrons are mainly confined in the ZnO nanowires, and holes in the p-$Mg_{0.35}Zn_{0.65}O$ shell layer surround the nanowires while some of them can be injected into the nanowires. Then, the electrons confined in the nanowires will recombine with the injected holes from the p-$Mg_{0.35}Zn_{0.65}O$ shell layer to produce photons. Fig. 4(d) illustrates the distribution of the electric potential in the core–shell heterostructure. The electric potential variation occurs mainly at the ZnO/p-$Mg_{0.35}Zn_{0.65}O$ interface, which reveals that the electrons and holes will mainly recombine at the interface of the core–shell heterostructure. The relatively high crystalline quality of the nanowires may facilitate the occurrence of lasing, while the large surface of the nanowires may provide an arena for strong scattering that is necessary for random lasing.

To test the above speculation, a forward bias has been applied to the n-ZnO/p-$Mg_{0.35}Zn_{0.65}O$ structures, and obvious emission has been detected, the emission spectra of which are illustrated in Fig. 5. When the injection current is 10 mA, weak broad emission can be detected. The spectrum is composed of two bands, and the one at 398 nm can be attributed to the near band-edge (NBE) emission of ZnO, while the other band at around 500 nm is usually attributed to the deep-level emission of ZnO.[34,35] When the injection current

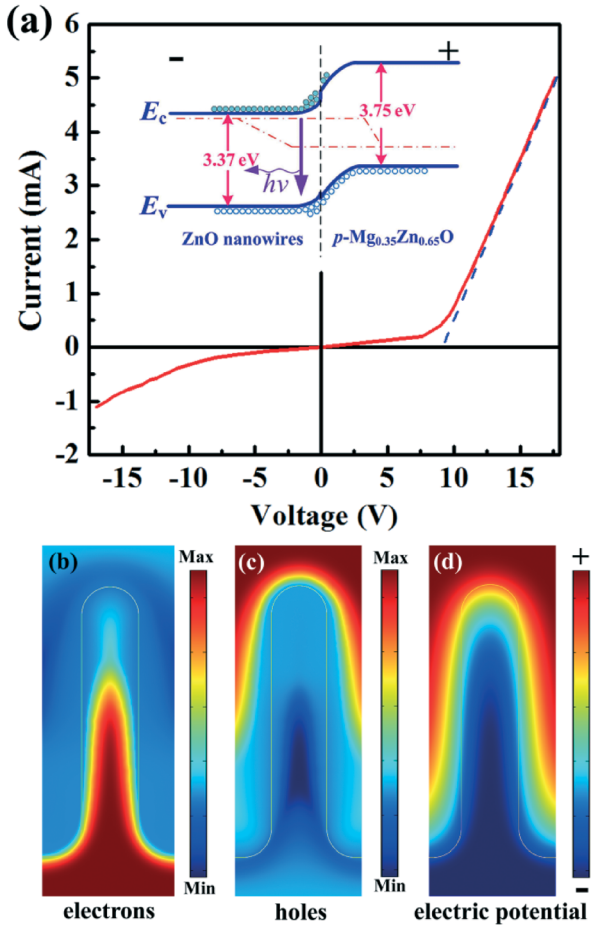

Fig. 4 (a) *I–V* curve of the p–n heterostructure (the inset shows the bandgap diagram under forward bias); (b) the electron distribution, (c) hole distribution and (d) electric potential distribution in the core–shell nanowire heterostructure.

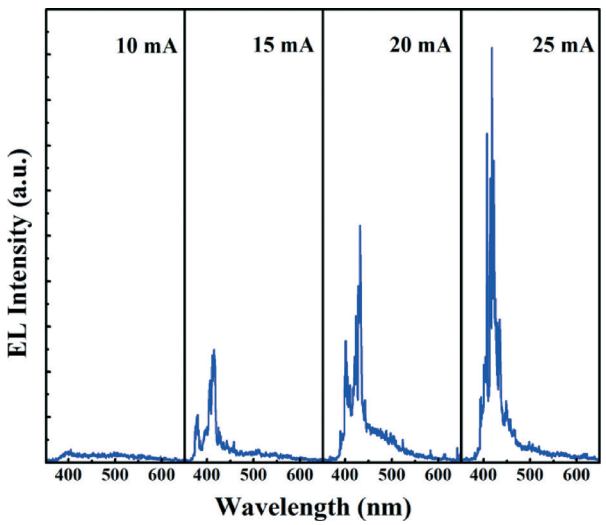

Fig. 5 Room temperature EL spectra of the heterostructure at different injection currents.

is increased to 15 mA, the intensity of the NBE emission is enhanced significantly, and some sharp peaks appear superposed on the broad spontaneous emission. When the injection current is increased further, the intensity of the sharp peaks increases greatly, and the FWHM of the sharp peaks is around 1.3 nm. The above phenomenon has been frequently observed in ZnO MIS or p–n junction structures,[15,18,23,28] and has been attributed to the occurrence of electrically pumped random lasers. The proof supporting the formation of random lasing is that the emission shows multidirectional distribution, as indicated in Fig. 6. One can see that the spectra collected at different observation angles show different lasing peaks, which are typical characteristics of a random laser.[18,36] Note that although there have been some reports on ultraviolet emission in ZnO core–shell nanowire structures,[37–40] no report on electrically pumped random lasers in ZnO core–shell nanowire p–n heterostructures can be found before.

The mechanism of random lasing observed in our case can be understood as follows: according to the carrier and electric potential distribution shown in Fig. 4, the recombination of electrons and holes will occur at the interface of the ZnO/$Mg_{0.35}Zn_{0.65}O$ interface, and photons are mainly produced there. The photons will undergo multiple scattering when they come out of the nanowires. Under the effect of multiple scattering, photons may return to the nanowires where they are emitted, thus closed loops will be formed. When the injection current is small, the optical gain in the closed loops is smaller than the loss, thus only broad spontaneous emission can be observed from the structure, as shown in the spectrum with an injection current of 10 mA in Fig. 5. Whereas, at larger injection current, the gain in the closed loops may exceed the loss, thus lasing will be observed, as indicated by the spectra with injection currents of 15 mA and above in Fig. 5. Since the closed loops are formed randomly between the nanowires, the emission recorded from different angles shows different lasing spectra. Note that the threshold

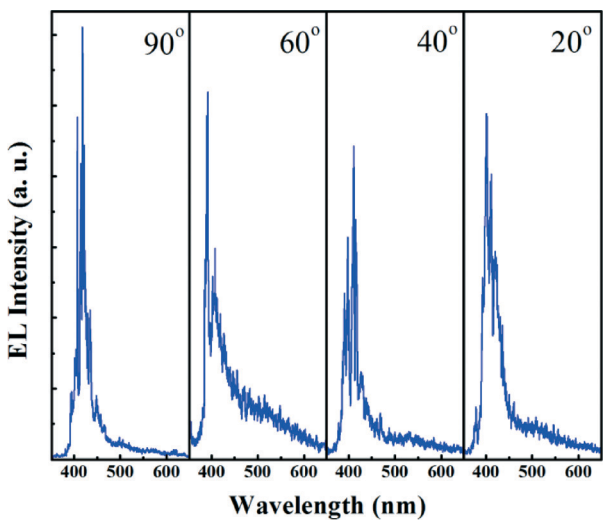

Fig. 6 Angular-dependent EL spectra of the device under an injection current of 25 mA, in which 90° means that the detector is perpendicular to the surface of the sample.

of the electrically pumped random lasers (around 15 mA) is smaller than the corresponding values ever reported in Au/SiO_x/ZnO or Au/MgO/ZnO MIS structures (usually around 70 mA)[15,22–24] and p–n homojunctions (~40 mA),[18] and the low threshold may originate from the relatively high crystalline quality of the nanowires and confinement of the carriers in the heterostructures.

Conclusions

In conclusion, n-ZnO/p-$Mg_{0.35}Zn_{0.65}O$ core–shell nanowire heterostructures have been fabricated, and random lasing has been observed from the structure under injection of a continuous current. A threshold of around 15 mA has been achieved, which is smaller than the corresponding values ever reported in similar MIS and p–n junction structures, and the small threshold has been attributed to the relatively high crystalline quality of the nanowires as well as carrier confinement in the heterostructures. The results reported in this paper reveal that nanowire core–shell p–n heterostructures may be a promising structure for electrically pumped random lasers.

Acknowledgements

This work is financially supported by the National Basic Research Program of China (2011CB302005), the National Science Foundation for Distinguished Young Scholars of China (61425021) and the Natural Science Foundation of China (11374296, 61475153, and 61177040).

Notes and references

1 S. Gottardo, S. Cavalieri, O. Yaroshchuk and D. Wiersma, *Phys. Rev. Lett.*, 2004, **93**, 263901.
2 Q. Song, Z. Xu, S. H. Choi, X. Sun, S. Xiao, O. Akkus and Y. L. Kim, *Biomed. Opt. Express*, 2010, **1**, 1401–1407.
3 Q. Song, S. Xiao, Z. Xu, V. M. Shalaev and Y. L. Kim, *Opt. Lett.*, 2010, **35**, 2624–2626.
4 D. S. Wiersma and S. Cavalieri, *Nature*, 2001, **414**, 708–709.
5 B. Redding, M. A. Choma and H. Cao, *Nat. Photonics*, 2012, **6**, 355–359.
6 B. Redding, G. Allen, E. R. Dufresne and H. Cao, *Appl. Opt.*, 2013, **52**, 1168–1172.
7 H. Cao, Y. G. Zhao, H. C. Ong, S. T. Ho, J. Y. Dai, J. Y. Wu and R. P. H. Chang, *Appl. Phys. Lett.*, 1998, **73**, 3656–3658.
8 H. C. Hsu, C. Y. Wu and W. F. Hsieh, *J. Appl. Phys.*, 2005, **97**, 064315.
9 J. Fallert, R. J. B. Dietz, M. Hauser, F. Stelzl, C. Klingshirn and H. Kalt, *J. Lumin.*, 2009, **129**, 1685–1688.
10 H. Y. Yang, S. F. Yu, H. K. Liang, C. Pang, B. Yan and T. Yu, *J. Appl. Phys.*, 2009, **106**, 043102.
11 M. H. Huang, S. Mao, H. Feick, H. Q. Yan, Y. Y. Wu, H. Kind, E. Weber, R. Russo and P. D. Yang, *Science*, 2001, **292**, 1897–1899.
12 R. Chen, Q. L. Ye, T. He, V. D. Ta, Y. Ying, Y. Y. Tay, T. Wu and H. Sun, *Nano Lett.*, 2013, **13**, 734–739.
13 T. M. Weng, T. H. Chang, C. P. Lu, M. L. Lu, J. Y. Chen, S. H. Cheng, C. H. Nieh and Y. F. Chen, *ACS Photonics*, 2014, **1**, 1258–1263.
14 H. Zhu, C. X. Shan, B. Yao, B. H. Li, J. Y. Zhang, Z. Z. Zhang, D. X. Zhao, D. Z. Shen, X. W. Fan, Y. M. Lu and Z. K. Tang, *Adv. Mater.*, 2009, **21**, 1613–1617.
15 H. Zhu, C. X. Shan, J. Y. Zhang, Z. Z. Zhang, B. H. Li, D. X. Zhao, B. Yao, D. Z. Shen, X. W. Fan, Z. K. Tang, X. Hou and K. L. Choy, *Adv. Mater.*, 2010, **22**, 1877–1881.
16 D. Vanmaekelbergh and L. K. van Vugt, *Nanoscale*, 2011, **3**, 2783–2800.
17 Q. Jiang, H. Zheng, J. Wang, H. Long and G. Fang, *ACS Appl. Mater. Interfaces*, 2012, **4**, 7043–7046.
18 J. Huang, S. Chu, J. Y. Kong, L. Zhang, C. M. Schwarz, G. P. Wang, L. Chernyak, Z. H. Chen and J. L. Liu, *Adv. Opt. Mater.*, 2013, **1**, 179–185.
19 P. D. García and C. López, *J. Mater. Chem. C*, 2013, **1**, 7357–7362.
20 C. Y. Liu, H. Y. Xu, J. G. Ma, X. H. Li, X. T. Zhang, Y. C. Liu and R. Mu, *Appl. Phys. Lett.*, 2011, **99**, 063115.
21 X. Y. Liu, C. X. Shan, S. P. Wang, Z. Z. Zhang and D. Z. Shen, *Nanoscale*, 2012, **4**, 2843–2846.
22 Q. Qiao, C. X. Shan, J. Zheng, H. Zhu, S. F. Yu, B. H. Li, Y. Jia and D. Z. Shen, *Nanoscale*, 2013, **5**, 513–517.
23 X. Y. Ma, J. W. Pan, P. L. Chen, D. S. Li, H. Zhang, Y. Yang and D. R. Yang, *Opt. Express*, 2009, **17**, 14426–14433.
24 X. Y. Ma, P. L. Chen, D. S. Li, Y. Y. Zhang and D. R. Yang, *Appl. Phys. Lett.*, 2007, **91**, 251109.
25 H. K. Liang, S. F. Yu and H. Y. Yang, *Appl. Phys. Lett.*, 2010, **96**, 101116.
26 H. K. Liang, S. F. Yu and H. Y. Yang, *Appl. Phys. Lett.*, 2010, **97**, 241107.
27 S. Chu, M. Olmedo, Z. Yang, J. Y. Kong and J. L. Liu, *Appl. Phys. Lett.*, 2008, **93**, 181106.
28 J. Y. Kong, S. Chu, Z. Zuo, J. J. Ren, M. Olmedo and J. L. Liu, *Appl. Phys. A: Mater. Sci. Process.*, 2012, **107**, 971–975.
29 J. Huang, M. M. Morshed, Z. Zuo and J. L. Liu, *Appl. Phys. Lett.*, 2014, **104**, 131107.
30 F. Sun, C. X. Shan, B. H. Li, Z. Z. Zhang, D. Z. Shen, Z. Y. Zhang and D. Fan, *Opt. Lett.*, 2011, **36**, 499–501.
31 J. S. Liu, C. X. Shan, H. Shen, B. H. Li, Z. Z. Zhang, L. Liu, L. G. Zhang and D. Z. Shen, *Appl. Phys. Lett.*, 2012, **101**, 011106.
32 J. S. Liu, C. X. Shan, B. H. Li, Z. Z. Zhang, K. W. Liu and D. Z. Shen, *Opt. Lett.*, 2013, **38**, 2113–2115.
33 Y. J. Lu, C. X. Shan, M. M. Jiang, B. H. Li, K. W. Liu, R. G. Li and D. Z. Shen, *RSC Adv.*, 2014, **4**, 16578–16582.
34 P. K. Shrestha, Y. T. Chun and D. P. Chu, *Light: Sci. Appl.*, 2015, **4**, e259.
35 Y. Zhu, A. Apostoluk, S. B. Liu, S. Daniele and B. Masenelli, *J. Semicond.*, 2013, **34**, 053005.
36 Z. F. Shi, Y. T. Zhang, X. C. Xia, W. Zhao, H. Wang, L. Zhao, X. Dong, B. L. Zhang and G. T. Du, *Nanoscale*, 2013, **5**, 5080–5085.

37 G. Grinblat, F. Bern, J. Barzola-Quiquia, M. Tirado, D. Comedi and P. Esquinazi, *Appl. Phys. Lett.*, 2014, **104**, 103113.
38 X. Y. Liu, C. X. Shan, C. Jiao, S. P. Wang, H. F. Zhao and D. Z. Shen, *Opt. Lett.*, 2014, **39**, 422–425.
39 W. Z. Liu, Y. Liang, H. Y. Xu, L. L. Wang, X. T. Zhang, Y. C. Liu and S. K. Hark, *J. Phys. Chem. C*, 2010, **114**, 16148–16152.
40 X. Mo, G. Fang, H. Long, S. Li, H. Wang, Z. Chen, H. Huang, W. Zeng, Y. Zhang and C. Pan, *Phys. Chem. Chem. Phys.*, 2014, **16**, 9302–9308.

